Journal of Molecular Catalysis A: Chemical 353–354 (2012) 148–155

Contents lists available at SciVerse ScienceDirect

Journal of Molecular Catalysis A: Chemical

journal homepage: www.elsevier.com/locate/molcata

Selective hydrogenation of citral to unsaturated alcohols over mesoporous Pt/Ti–Al_2O_3 catalysts. Effect of the reduction temperature and of the Ge addition

Tchirioua Ekou[a,b], Aurélien Flura[a], Lynda Ekou[b], Catherine Especel[a,*], Sébastien Royer[a]

[a] Department of Chemistry, LACCO UMR 6503, University of Poitiers, 4 rue Michel Brunet, 86022 Poitiers Cedex, France
[b] Laboratoire de Thermodynamique et de Physico-Chimie du Milieu University of Abobo-Adjamé, 02 Bp 801, Abidjan 02, Cote d'Ivoire

ARTICLE INFO

Article history:
Received 26 August 2011
Received in revised form
14 November 2011
Accepted 14 November 2011
Available online 22 November 2011

Keywords:
Mesoporous composite
Platinum
Titania
Germanium
Citral hydrogenation
SMSI effect

ABSTRACT

Pt/*y*%Ti–Al_2O_3 (*y* corresponding to the atomic percent of Ti in alumina, in the range 10–33%), and derived bimetallic Pt-Ge/10%Ti–Al_2O_3 nanocomposite catalysts were synthesized, characterized, and reduced either at 300 °C and 500 °C (this latter temperature being performed in order to generate strong metal–support interactions, *i.e.* a SMSI effect). The materials were characterized in detail with techniques including elemental analysis, X-ray diffraction (XRD), high-resolution transmission electron microscopy (HRTEM) and nitrogen physisorption to evaluate their structural and textural properties. Due to the templating approach used, well-defined mesopore structures with high surface areas and mesopore volumes are obtained for all materials. The SMSI effect, evaluated using a structure insensitive model reaction, *i.e.* the cyclohexane dehydrogenation, is observed to be more pronounced on the Pt/*y*%Ti–Al_2O_3 catalysts with *y* = 20 and 33% than on a Pt/TiO_2 P25 (Degussa P25 titania) sample, showing the beneficial effect of Ti fine dispersion through incorporation in alumina matrix on the generated metal–support interaction. During citral hydrogenation reaction, the selectivity toward unsaturated alcohols (UA: nerol and geraniol) is related to Ti and/or Ge loadings on the nanocomposite, as well as reduction temperature. Both SMSI effect and Ge addition promote the UA selectivity leading to similar values than on Pt/TiO_2 P25 sample.

1. Introduction

According to the IUPAC (International Union of Pure and Applied Chemistry) definition, porous materials can be classified into three groups: (i) microporous materials, presenting pore diameters lower than 2 nm, (ii) mesoporous materials possessing pore diameters ranged from 2 to 50 nm, and (iii) macroporous materials having pore diameters larger than 50 nm [1]. The preparation of ordered mesoporous materials has recently attracted much more people's attention and many efforts were performed to develop surfactant-templated synthesis of mesostructured inorganic/surfactant composites, and especially for non siliceous oxides that can find easy use as support for heterogeneous catalysis [2–6]. The great interest for mesoporous materials is explained by their special textural features: uniform channel, large surface area, narrow pore size distribution, tunable pore size in a wide range of mesopore size, and so on. These systems lead to wide applications in the fields of catalysis, separation, electromagnetics, photoelectronics and as host for nanosynthesis [7–9]. Among the family of mesoporous materials, the synthesis of hexagonal silica as well mesoporous alumina has attracted considerable attention over the past few years [10,11]. In order to modify the catalytic activity of the mesoporous materials, several other metal ions were incorporated into the framework or grafted on the surface, such as Ti, V, Mn or Sn [12–14]. The catalytic behavior is strongly influenced by the nature, the local environment and the stability of the metal introduced.

Recently, we evaluated the catalytic properties of Pt supported on Ti-doped mesoporous silica nanocomposites, using the structure insensitive reaction of cyclohexane dehydrogenation [15]. This study was performed in order to determine the effect of the support morphological properties on the strong metal–support interaction (SMSI effect occurring over a reducible oxide support as TiO_2). We evidenced that the titania crystal size is a determining parameter allowing a control of the SMSI effect: the metal–support interaction being stronger for the lower crystal size.

The present study focuses on the preparation of Pt/Ti–Al_2O_3 mesoporous catalysts by direct addition of titanium precursor before alumina condensation, in order to incorporate the modifying element into the Al_2O_3 structure. These systems were evaluated for the liquid phase hydrogenation of an α,β-unsaturated aldehyde, in order to form selectively α,β-unsaturated alcohols which constitute important intermediates for various industrial applications [16]. The selective hydrogenation of carbonyl groups of α,β-unsaturated aldehydes is a challenging step since the hydrogenation of C=C bonds is thermodynamically favored over the C=O bond's one [17]. In this research field, 3,7-dimethyl-2,6-octadienal

* Corresponding author. Tel.: +33 5 4945 3994; fax: +33 5 4945 3741.
E-mail address: catherine.especel@univ-poitiers.fr (C. Especel).

1381-1169/$ – see front matter © 2011 Elsevier B.V. All rights reserved.
doi:10.1016/j.molcata.2011.11.018

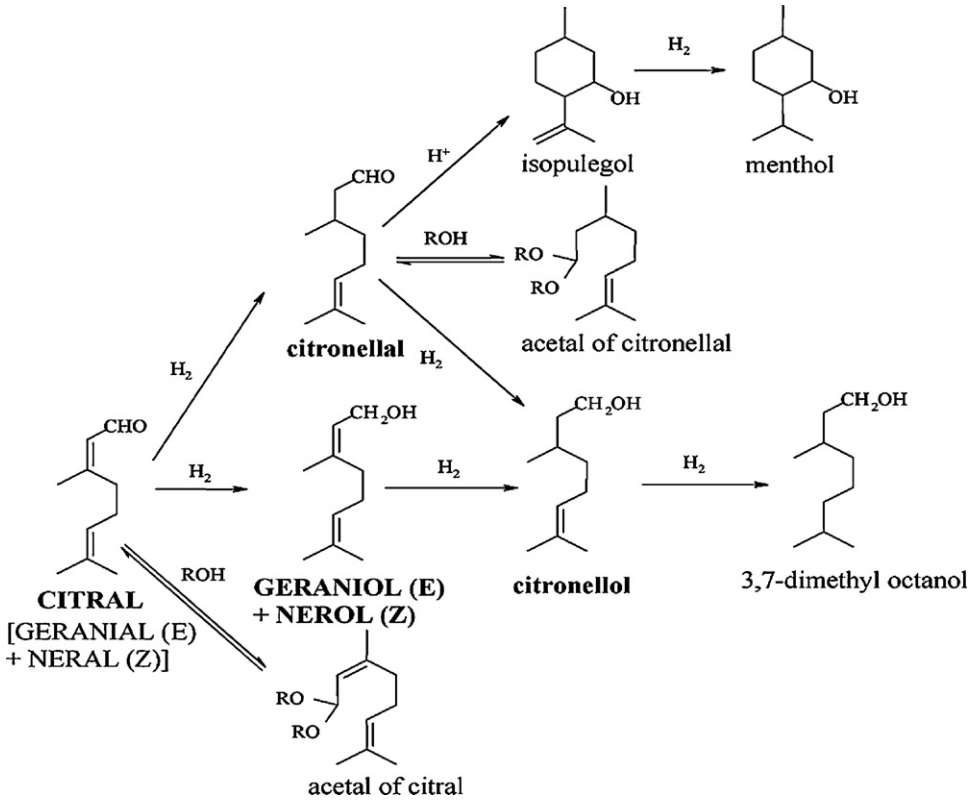

Scheme 1. Reaction scheme for citral hydrogenation.

(*i.e.* citral) is frequently used as a probe α,β-unsaturated aldehyde, presenting conjugated C=O and C=C bonds and an isolated C=C bond. The reaction pathways of citral hydrogenation are complex, leading to a variety of products such as citronellal, citronellol, geraniol, nerol, menthol, and others through hydrogenation reactions involving C=C and C=O bonds (Scheme 1). Nevertheless, the hydrogenation of the carbonyl group is of great interest to form the unsaturated alcohols (UA), *i.e.* nerol and geraniol, the most valuable products for the food, pharmaceutical, and cosmetic industries [18–20]. Apart from these main reactions, secondary processes of cyclization or of reaction with the solvent (alcohol) can lead to other by-products like isopulegols or acetals, respectively. We previously studied the catalytic performances of Pt/TiO_2 catalysts for citral hydrogenation, and concluded that the UA selectivity, *i.e.* the C=O bond activation, can be promoted by (i) a reduction at high temperature to generate SMSI effect, and (ii) the modification of Pt by Ge addition generating bimetallic interactions [21,22]. In the literature, only few studies reported the hydrogenation of α,β-unsaturated aldehydes over nanocomposite catalysts [23,24]. Consequently, in this paper, high surface area $Ti–Al_2O_3$ materials were used as potential mesoporous support to further impregnate Pt metallic precursor, to replace classical alumina support. The oxides were synthesized via a sol–gel based mesostructuration procedure to generate titania nanodomains in the Al_2O_3 porosity. After Pt impregnation and thermal activation, the as-synthesized mesoporous systems were evaluated in citral hydrogenation reaction performed at 70 °C under hydrogen pressure (7 MPa), as well for the gas phase cyclohexane dehydrogenation. Several techniques were used in combination to characterize mesoporous materials, in order to provide unambiguous structural information.

Our objectives consist in studying: (i) the feasibility of the $Ti–Al_2O_3$ mesoporous synthesis, (ii) the potential of these modified supports to generate improved SMSI effect, and (iii) the influence of the Ge addition on the catalytic performances of $Pt/Ti–Al_2O_3$ systems in order to maximize UA selectivity.

2. Experimental

2.1. Catalyst preparation

All chemicals were used as received without further treatment. The preparation of the $y\%Ti–Al_2O_3$ mesoporous supports was performed in order to substitute a given atomic percentage of Al^{3+} cations by Ti^{4+} cations. In this study, this percentage is noted $y\%$ and corresponds to the ratio $\%_{atom}Ti/(\%_{atom}Ti + \%_{atom}Al)$. The $y\%Ti–Al_2O_3$ oxides (y = 0, 10, 20 and 33%) were synthesized as follows: the alumina precursor (aluminum sec-butoxide, 97%, Alfa Aesar) was dissolved in 1-butanol (ButOH) at 65 °C and stirred until complete dissolution. The same procedure was carried out in parallel with the cationic surfactant ((1-hexadecyl) trimethylammonium bromide, CTABr, 98%, Alfa Aesar). The two solutions were then mixed and kept at 65 °C under stirring. Thereafter, the titania precursor (titanium isopropoxide) previously dissolved in a hot solution of 1-butanol under vigorous stirring is added slowly. After 10 min of vigorous stirring, a limited amount of water was added in order to start the hydrolysis of the alumina precursor. The molar composition of the mixture was $0.5CTABr:1Al^{3+}:10ButOH:2H_2O$. Stirring was maintained for 4 h at 65 °C until homogeneous gel was obtained. Thereafter, the gel was autoclaved at 100 °C for 24 h under autogenous pressure and static condition. The product was washed several times with 1-butanol, before to be dried at room temperature during 24 h, and then at 80 °C during 24 h. Finally, the solid was calcined at 600 °C with a heating rate of 3 °C min^{-1}, and kept at this temperature for 4 h before use as support.

Monometallic 1.0 wt.% $Pt/y\%Ti–Al_2O_3$ catalysts were synthesized by an ion exchange method using H_2PtCl_6 as platinum source [25–27]. After impregnation, the catalysts were dried at 110 °C overnight, and then calcined for 4 h in flowing air at 400 °C. Finally, solids were reduced at 300 °C or 500 °C under pure hydrogen for 4 h. Pt-Ge/10%$Ti–Al_2O_3$ nanocomposite catalysts were prepared by addition of Ge modifier on the

Table 1
Physical properties of the 1.0 wt.% Pt/*y*%Ti–Al_2O_3 catalysts after reduction at 300 °C (r300) or 500 °C (r500).

Sample	Ti[a]/wt.%	Pt[a]/wt.%	Cl[a]/wt.%	S_{BET}/m^2 g^{-1}	D_p/nm	V_p/cm^3 g^{-1}	D_{Pt} [b]/nm
Al_2O_3	–	–	–	302	7.1	0.72	–
Pt/Al_2O_3 r300	0	1.0	1.2	289	6.8	0.67	0.85 ± 0.15
Pt/10%Ti–Al_2O_3 r300	7	1.0	1.0	321	6.0	0.40	0.85 ± 0.15
Pt/20%Ti–Al_2O_3 r300	13	1.0	0.8	265	4.2	0.32	0.85 ± 0.15
Pt/33%Ti–Al_2O_3 r300	21	0.9	0.9	258	4.1	0.30	0.85 ± 0.15
Pt/Al_2O_3 r500	0	0.9	0.8	282	6.8	0.65	0.90 ± 0.20
Pt/10%Ti–Al_2O_3 r500	7	1.0	0.5	284	6.1	0.40	0.90 ± 0.20
Pt/20%Ti–Al_2O_3 r500	13	1.0	0.5	215	4.2	0.25	0.90 ± 0.20
Pt/33%Ti–Al_2O_3 r500	21	0.9	0.4	215	4.2	0.26	0.90 ± 0.20
Pt/TiO_2 P25 r300	60	1.0	0.5	49	8.0	–	1.90 ± 0.20
Pt/TiO_2 P25 r500	60	1.0	<0.2	49	8.0	–	2.00 ± 0.20

[a] Evaluated using ICP.
[b] Evaluated using TEM.

monometallic 1.0 wt.% Pt/10%Ti–Al_2O_3 parent catalyst reduced at 300 °C. The addition was performed by surface redox reaction between dissociatively adsorbed hydrogen on accessible platinum and the germanium salt ($GeCl_4$) dissolved in water ("catalytic reduction" method described precisely in previous studies [25,28]). Finally, the bimetallic nanocomposites were reduced for 1 h (2 °C min^{-1} heating rate) at 300 °C.

2.2. Catalysts characterization

Specific surface area, pore size distribution and pore volume were obtained from N_2-adsoption desorption isotherms collected on a TRISTAR instrument from Micromeritics. Samples were degassed for 1 night at 300 °C under 0.15 mbar before experiments to ensure a clean and dry material. The specific surface area, S_{BET}, was determined from the linear part of the BET plot. The mesopore size distribution was determined by the non local density functional theory (NLDFT) method and calculated using the Autosorb-1 1.52 software. The kernel selected was N_2 on silica assuming cylindrical pore geometry and the equilibrium based on the desorption branch. Pore volume is determined on the isotherms at $P/P_0 = 0.97$.

Powder X-ray diffraction (XRD) patterns were collected on a Bruker AXS D5005 X-ray diffractometer, using a CuKα radiation (λ = 1.54184 Å) as X-ray source. The signal was recorded for 2θ comprised between 10° and 80° with a step of 0.05° (step time of 2 s). Phase identification was made by comparison with JCPDS database.

Transmission electron microscopy (TEM) studies were performed on a JEOL 2100 UHR instrument (operated at 200 kV with a LaB_6 source and equipped with a Gatan Ultra scan camera). All the samples were embedded in a polymeric resin (spurr) and cut into a section as small as 50 nm using an ultramicrotome equipped with a diamond knife. Cuts were then deposited on a Cu grid holey carbon film. Average metal particle sizes (given in Table 1) were determined by measuring at least 100 particles for each analyzed sample, from at least 5 different micrographs.

2.3. Cyclohexane dehydrogenation

The probe reaction of cyclohexane dehydrogenation was carried out under atmospheric pressure in a continuous flow reactor at 270 °C according to experimental protocol described elsewhere [21]. The catalyst (20 mg) was first activated under H_2 flow (60 mL min^{-1}) at the desired temperature for 1 h (300 °C or 500 °C) and then cooled to the reaction temperature (270 °C). Analysis of the reaction products was performed by gas chromatography equipped with a flame ionization detector (Varian 3400×) and a HP-PLOT Al_2O_3 "KCl" column for separation. Benzene was the only detected product.

2.4. Citral hydrogenation

The liquid phase hydrogenation of citral was carried out in a 300 mL stirred autoclave (Autoclave Engineers, fitted with a system for liquid sampling) at 70 °C and at constant pressure of 7 MPa, following the same experimental conditions applied in previous studies [22,25,28]. Before each catalytic experiment, the catalyst (400 mg) was reduced at the desired temperature for 1 h (300 °C or 500 °C), then immersed into 90 mL of solvent (isopropanol 99%) without exposure to air before the transfer toward the autoclave. Liquid samples were analyzed by gas chromatography on a Thermofinnigan gas chromatograph equipped with a FID detector and a capillary column DB-WAX (J&W, 30 m, 0.53 mm i.d.) using nitrogen as carrier gas.

3. Results and discussion

3.1. Characterization of the catalysts

1.0 wt.% Pt/*y*%Ti–Al_2O_3 nanocomposite samples were prepared with various Ti atomic concentrations (*y* = 10, 20, and 33%). After synthesis of the support and platinum deposition, the materials were reduced either at low (300 °C) or high (500 °C) reduction temperature. All the as-synthesized monometallic catalysts are listed in Table 1 with their main physical properties. A 1.0 wt.% Pt/TiO_2 P25 (Degussa P25 titania) catalyst, prepared and activated in the same way, *i.e.* by impregnation of the same precursor salt (H_2PtCl_6) and finally reduced at 300 °C or 500 °C, is also given in Table 1 in order to compare the properties of the Pt/*y*%Ti–Al_2O_3 systems with a reference sample supported on bulk titania.

Fig. 1 shows the wide-angle XRD ($10° < 2\theta < 80°$) patterns. The alumina sample calcined at 600 °C presents the reflections characteristic of the γ-Al_2O_3 phase as often reported in the literature for alumina materials calcined at similar temperatures. The further impregnation of platinum, followed by calcination and reduction (at 300 °C or 500 °C), does not result in any structural modification of the alumina support. Indeed, the γ-Al_2O_3 phase is always observed, while no supplementary reflection attributable to either Pt^0 or PtO can be observed. This suggests a satisfying dispersion of the metallic phase.

The insertion of the Ti atoms in the alumina structure leads to a progressive decrease in γ-Al_2O_3 reflection intensity. Nevertheless, no crystallized titania phase (anatase, brookite or rutile) can be detected by X-ray diffraction, even at 33 at.% of Ti. This result suggests a satisfying incorporation of the titanium atoms in the alumina structure, accompanied with a progressive loss of the crystalline character of the alumina which will remain amorphous even after calcination at 600 °C.

Nitrogen adsorption–desorption isotherms of the mesostructured Ti–Al_2O_3 and derived noble metal catalysts are presented in

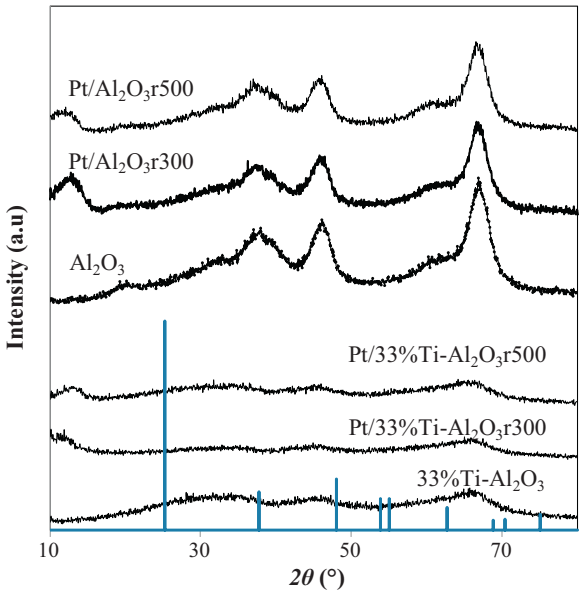

Fig. 1. X-ray diffraction patterns obtained on the y%Ti–Al_2O_3 supports and respective 1.0 wt.% Pt/y%Ti–Al_2O_3 (y = 0 and 33) catalysts reduced at 300 °C and 500 °C. Vertical bars: TiO_2 anatase phase (JCPDS file no.: 089-4920).

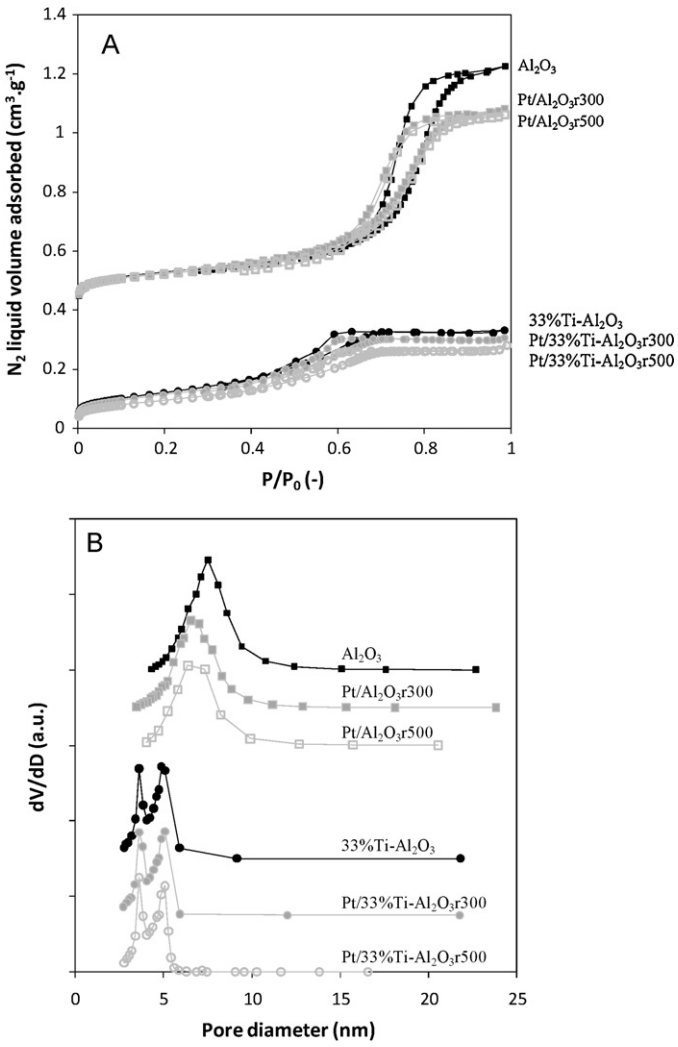

Fig. 2. N_2 adsorption–desorption curves (A) and corresponding NLDFT pore size distribution (B) obtained over the y%Ti–Al_2O_3 nanocomposites and respective 1.0 wt.% Pt/y%Ti–Al_2O_3 (y = 0 and 33) based catalysts reduced at 300 °C and 500 °C.

Fig. 2A. All the samples exhibit type IV isotherm [29]. Sharp adsorption and desorption steps followed by a plateau at high P/P_0, which is characteristic of capillary condensation and evaporation in the mesopores, are clearly observed [30]. While a hysteresis loop close to H1-type according to the IUPAC classification [29] is observed for the alumina materials, the hysteresis loop is changing with the titanium incorporation. Then, evolution from H1-type to H2-type is observed (Fig. 2A). Nevertheless, materials always present porosity in the mesopore range. The absence of any sharp rise in the nitrogen uptake as P/P_0 close to 1 also tends to conclude on a homogeneous pore size repartition, without large mesopore or macropore in the support [31,32].

The textural properties of the Pt-based catalysts are gathered in Table 1, since the impregnation–calcination–reduction cycle of 1.0 wt.% of Pt does not induce any important modification of the physical properties (either pore size, pore volume or surface area). The limited modifications (in all case <4%) are easily attributed to the low noble metal content and the small generated Pt particle sizes. While the insertion of 10% of Ti in the alumina support leads to slight increase in surface area (~10%), compared to this obtained for the alumina (Table 1), a further increase of the Ti content in the solid leads to a progressive decrease of the BET surface area (S_{BET}). Nevertheless, the surface areas remain in all cases higher than 250 $m^2\ g^{-1}$. In addition, pore size (D_p) and pore volume (V_p) (Table 1) are observed to decrease with the increase in Ti content. While the Pt/Al_2O_3 material presents a surface area of 289 $m^2\ g^{-1}$ after reduction at 300 °C, Pt/33%Ti–Al_2O_3 material presents a surface area of 258 $m^2\ g^{-1}$. The decrease of the pore volume is more marked, with a decrease of 55% of the value between these two materials. Nevertheless, this evolution (limited surface area decrease, more important decrease in pore volume) is consistent since pore diameter is decreasing from 6.8 nm to 4.1 nm (Table 1, Fig. 2B). The surface areas of the titania-containing materials are decreasing of about 16% by increasing the reduction temperature from 300 °C to 500 °C, whereas the decrease is rather limited for the Pt/Al_2O_3 catalysts (Table 1). Nevertheless, compared to the classical Pt/TiO_2 P25 reference system, all the Pt/Ti–Al_2O_3 catalysts still display high specific surface area ($215 \le S_{BET} \le 321\ m^2\ g^{-1}$) and mesopore volume ($0.25 \le V_p \le 0.67\ cm^3\ g^{-1}$).

TEM analysis was performed in order to study the homogeneity in the distribution of titanium and platinum in the Pt/y%Ti–Al_2O_3 mesoporous materials. Representative TEM images of the Pt/Al_2O_3 and Pt/33%Ti–Al_2O_3 catalysts after reduction at 300 °C and 500 °C are presented in Fig. 3, while TEM images for the reference Pt/TiO_2 P25 catalyst can be found elsewhere [33]. TEM images show that the materials present an aggregate-like morphology. Thus the porosity is generated by the arrangement of the elementary particles inside these aggregates. This porosity intra-aggregate is observed whatever the titanium content and activation conditions (Fig. 3A and C). Indeed, the pore structure is still present on the Pt/33%Ti–Al_2O_3 whatever the reduction temperature (Fig. 3E and F). The platinum particles are clearly observed (Fig. 3B–F), and particle sizes obtained after analysis of characteristic TEM images for all considered samples are summarized in Table 1. It seems from TEM analysis that the titanium content does not affect the platinum dispersion, since measured sizes are always ranged between 0.7 nm and 1.1 nm (Table 1). These sizes are two times lower than those measured over the Pt/TiO_2 P25 reference material, showing the beneficial effect of the support physical properties on the noble metal dispersion. In addition to the noble metal particles, some crystallized particles are detected in the titania-containing materials. These particles are rarely observed, and only in materials having high Ti content (33%, and in a lower extent 20%). EDXS analysis focused

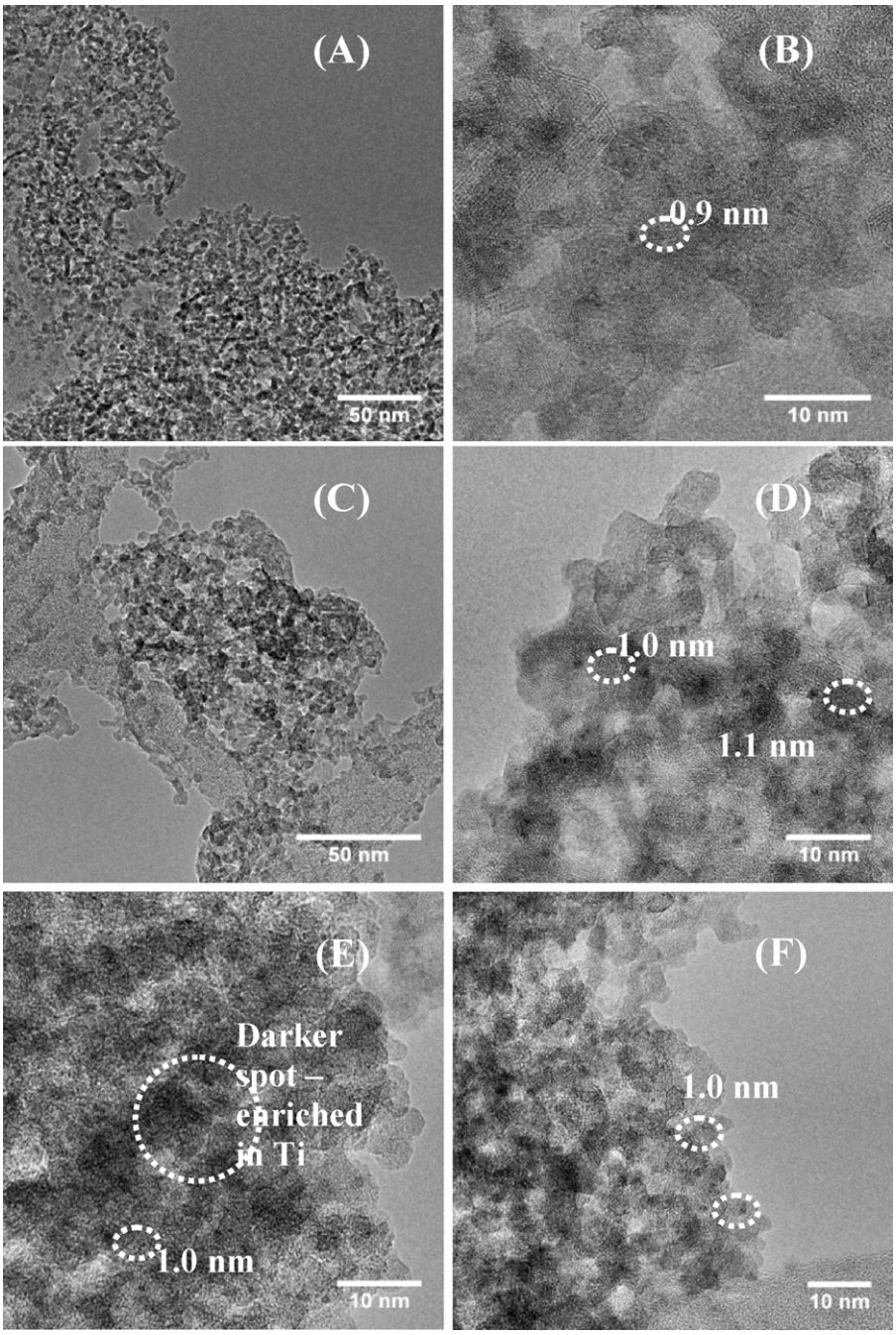

Fig. 3. TEM images of 1.0 wt.% Pt/Al_2O_3 catalysts reduced at 300 °C (A and B) and 500 °C (C and D), 1.0 wt.% $Pt/33\%Ti–Al_2O_3$ catalysts reduced at 300 °C (E) and 500 °C (F).

on these crystallized particles shows that these particles mainly contain titanium atoms, leading us to suppose the formation of some external anatase particles in these materials. Nevertheless, these particles are rarely observed, suggesting a limited formation of external phase, as confirmed by the lack in TiO_2 reflections on the XRD patterns whatever the titanium content and activation conditions. This result suggests that the solubility of titanium inside the alumina network is limited, and that the formation of external titania phase could not be completely excluded at high Ti content in $y\%Ti–Al_2O_3$.

To conclude, highly dispersed Pt particles form on the $y\%Ti–Al_2O_3$ materials, which can be attributed to the high reactivity of alumina surface toward metallic precursor species, *i.e.* to a good interaction between alumina and metal [34–36].

3.2. Cyclohexane dehydrogenation

The activity of the $Pt/y\%Ti–Al_2O_3$ materials was evaluated for the cyclohexane dehydrogenation, a structure insensitive probe reaction involving only the metallic phase [37–39]. The interaction between a catalytically inert atom (as titanium) and an active metal (as platinum) is suggested to greatly affect the apparent activity of the corresponding catalysts. The measured activity directly linked to the number of Pt surface active sites will allow consequently estimating the evolutions of the Pt accessibility, *i.e.* the interaction between titania and the active phase according the reduction temperature. The measured catalytic properties are given as function of titanium loading and reduction temperature in Table 2, in terms of specific activities (mol h^{-1} $g_{Pt}{}^{-1}$). First, the data reported in Table 2

Table 2
Specific activity of the monometallic 1.0 wt.% Pt/*y*%Ti–Al_2O_3 catalysts for cyclohexane dehydrogenation at 270 °C.

Sample Pt/	$T_{reduction}$/°C	A_s [a]/mol h^{-1} g_{Pt}^{-1}	R[b]
Al_2O_3	300	10.4	0.9
	500	11.9	
10%Ti–Al_2O_3	300	13.3	1.2
	500	11.3	
20%Ti–Al_2O_3	300	16.4	4.0
	500	4.1	
33%Ti–Al_2O_3	300	12.6	3.9
	500	3.2	
TiO_2 P25	300	17.2	1.5
	500	11.3	

[a] A_s value estimated with an error of 10%.
[b] $R = A_{s300}$ (after reduction at 300 °C)/A_{s500} (after reduction at 500 °C).

indicate that the specific activities of the Pt/Al_2O_3 catalyst reduced either at 300 °C or 500 °C are quite comparable (an experimental error of 10% having to be considered for the cyclohexane conversion rate and then for the specific activity values given in Table 2). This observation is in accordance with the similar Pt particle size observed previously from TEM analysis for the two monometallic Pt/Al_2O_3 catalysts whatever the reduction temperature.

After reduction at 300 °C, the specific activities obtained for the various catalysts can be classified as follows: Pt/TiO_2 P25 > Pt/*y*%Ti–Al_2O_3 > Pt/Al_2O_3. This evolution between these systems is not consistent with this of the Pt particle size since the Pt/TiO_2 P25 catalyst presents larger noble metal particles than other samples (1.9 nm compared to 0.85 nm, Table 1). The origin of these differences can be linked to the various acidities of the oxide supports, which can result partly from variations in the chlorine contents. Indeed, according to Table 1, for the catalysts reduced at 300 °C, the chlorine content evolves as following: Pt/TiO_2 P25 < Pt/*y*%Ti–Al_2O_3 < Pt/Al_2O_3, *i.e.* samples prepared on pure and modified alumina are more acidic than that synthesized on pure titania. In previous studies [40,41], a poisoning effect of chlorine has been observed during cyclohexane dehydrogenation, due to an alteration of the benzene desorption (benzene being the only product of the reaction). This behavior was explained by the inductive effect of the chlorine species involving modifications of the electronic properties of the metallic particles, and then resulting in a lower catalytic activity.

On the other hand, it can be seen from Table 2 that lower specific activities are obtained for all the Pt/*y*%Ti–Al_2O_3 catalysts after reduction at 500 °C compared to their counterparts reduced at 300 °C, despite similar Pt particle sizes for all these samples. Even by considering experimental error of 10% on the specific activities, this phenomenon is particularly observed for the two highest Ti contents (*y* = 20 and 33%), since the specific activities of these samples after reduction at 500 °C are around 4 times lower than those after reduction at 300 °C (see the *R* ratio in Table 2, defined as the ratio of the specific activities of a sample after reduction at 300 °C and 500 °C respectively). Such a decrease in activity is consistent with a strong metal–support interaction (SMSI effect) developed on the Pt/*y*%Ti–Al_2O_3 catalysts after reduction at high temperature. Indeed, the formation of $TiO_{(2-x)}$ species ($x < 2$) with the increase of the reduction temperature induces a coverage of a part of the metallic active surface, leading in-fine to a decrease in specific activity. The SMSI effect seems to be more important on the Pt/*y*%Ti–Al_2O_3 catalysts (with *y* = 20 and 33%) than on the 1.0 wt.% Pt sample supported on bulk TiO_2 P25, for which the specific activity decreases only by a 1.5 factor when the reduction temperature increases from 300 °C to 500 °C (*R* = 1.5, Table 2). This behavior is the same as one observed for previously studied Pt/TiO_2–SiO_2 materials, where the obtained results allowed concluding on a beneficial effect of the titania dispersion on the generated metal–support interaction [15].

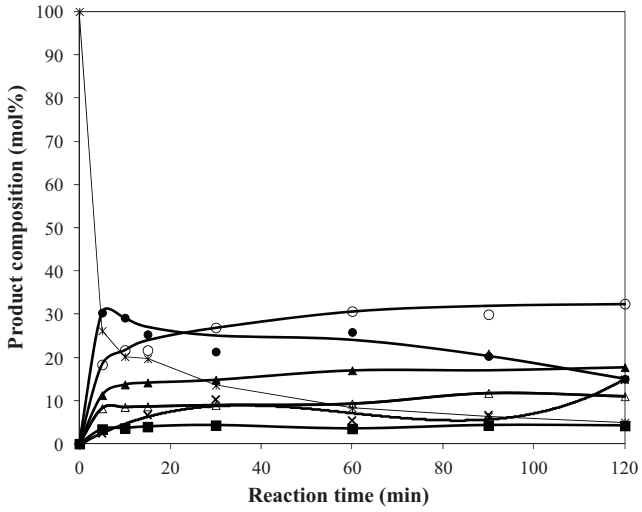

Fig. 4. Hydrogenation of citral on 1.0 wt.% Pt/Al_2O_3 catalyst reduced at 300 °C as function of time: citral (*); citronellal (●); citronellol (△); unsaturated alcohol (■); 3,7-dimethyl octanol (▲); isopulegol (×); others products (○).

3.3. Citral hydrogenation

The catalytic behavior of the Pt/Al_2O_3 sample for the liquid-phase hydrogenation of citral (70 °C, P_{H2} = 7 MPa) was evaluated after *in situ* reduction of the catalyst (at 300 °C or 500 °C) before test. The results obtained for the two reduction temperatures are quite similar, leading to temporal concentration profiles of the citral and main products as presented in Fig. 4 in the case of 300 °C as reduction temperature.

The reaction products are: citronellal, citronellol, geraniol and nerol (α,β-unsaturated alcohols, noted UA), 3,7-dimethyl octanol, isopulegol (obtained by citronellal cyclization) and a group of "others products" issue from side reactions, gathering acetals and menthol together. The high proportion of "others products" + isopulegol is explained by the fact that the Pt/Al_2O_3 catalyst possesses surface acid sites necessary for the formation of these by-products via acid catalyzed processes. Notably, previous studies reported in the literature have mentioned that the presence of remaining chlorine species on the catalyst can contribute to induce surface acidity [42]. In the present work, it must be recall that the preparation of the Pt/Al_2O_3 catalyst is performed from a chloride precursor (H_2PtCl_6), leading to a non negligible chlorine content (Table 1).

On the Pt/TiO_2 P25 catalyst prepared from the same precursor salt, the formation of isopulegol and "others products" is also observed (the temporal concentration profiles for this sample being published previously [33]).

The hydrogenation of citral on the Pt/Al_2O_3 catalyst takes place rapidly during the first 5 min, a conversion of 74% being reached at that point (Fig. 4). However an apparent decrease in the rate of citral consumption is observed at longer reaction times, which must be partly due to a catalyst deactivation. However, under the experimental conditions (*i.e.* reaction performed in a batch reactor), it is quite logical that the rate drops with reaction progress since the citral concentration decreases continuously in the autoclave. On the other hand, the formation of various reaction products leads to an adsorption competition between reactant and products that may limit the citral conversion with time. Nevertheless, a similar evolution of the temporal reactant curve was observed previously for citral hydrogenation over various SiO_2-supported noble metals

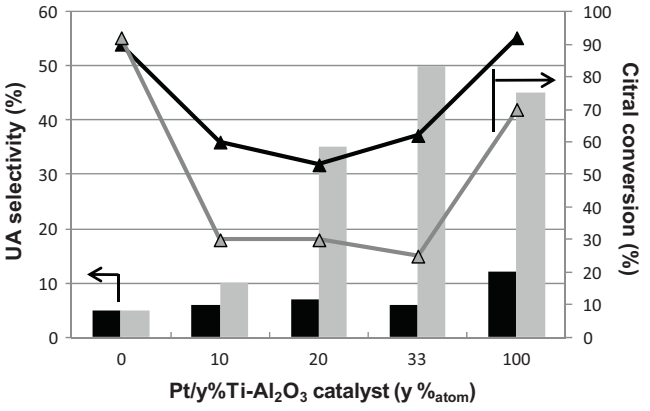

Fig. 5. Citral conversion after 60 min reaction time and selectivity to unsaturated alcohols at 40% citral conversion on the 1.0 wt.% Pt/*y*%Ti–Al_2O_3 monometallic catalysts reduced at 300 °C (black) and at 500 °C (grey). Conversion and selectivity values are estimated with an error of 10%.

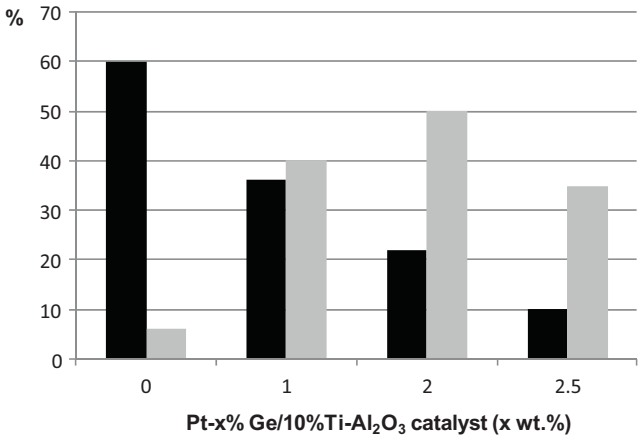

Fig. 6. Citral conversion after 60 min reaction time (black) and selectivity to unsaturated alcohols at 40% citral conversion (grey) on the 1.0 wt.% Pt–*x* wt.% Ge/10%Ti–Al_2O_3 bimetallic catalysts reduced at 300 °C. Conversion and selectivity values are estimated with an error of 10%.

[43–45], as well as by Rodriguez and Bueno during crotonaldehyde hydrogenation in gas phase over Co/SiO_2 catalysts [46]. The generally proposed explanation of this behavior, based on several kinetic and spectroscopic studies, is a decomposition of the citral or unsaturated alcohols yielding to irreversible chemisorbed CO and carbonaceous species that accumulate on the catalyst surface and block a fraction of the active sites [43,47,48].

Finally, the formation of the intended products (unsaturated alcohols, *i.e.* nerol and geraniol) is very low whatever the reduction temperature, indicating that the C=C/C=O adsorption competition of the citral molecules is mainly in favor of the C=C bond over alumina supported platinum catalysts.

Fig. 5 displays the citral conversion after 60 min reaction time and the UA selectivity at citral isoconversion (40%) for each Ti-containing catalyst, compared with the Pt samples supported on pure alumina (*y* = 0%) and pure titania (*y* = 100%) respectively. Fig. 5 shows a decrease in citral conversion over the Pt/*y*%Ti–Al_2O_3 catalysts, whatever the titanium content and reduction temperature. For the catalyst series reduced at 300 °C, this behavior was not observed previously during the probe reaction of cyclohexane dehydrogenation, showing the difficulty to compare catalytic behaviors in different reaction media (gas phase and liquid phase). Fig. 5 indicates that the conversion decrease is twice higher for the Ti-containing catalysts after reduction at 500 °C. This phenomenon cannot result from a variation of the Pt particle sizes, since the TEM study suggests comparable particle sizes for the Pt/*y*%Ti–Al_2O_3 catalysts reduced at 300 °C and 500 °C (Table 1). This evolution can then be related to the SMSI effect, with the reduction of titania species ($TiO_{(2-x)}$ ($x < 2$) species) which can cover a part of the Pt surface after reduction at 500 °C. A conversion decrease is also observed for the Pt/TiO_2 P25 sample after reduction at 500 °C. Nevertheless, this decrease in activity is largely lower, suggesting a lower SMSI effect over Pt/TiO_2 P25 compared to the Pt/*y*%Ti–Al_2O_3 systems. Then, the Pt/TiO_2 P25 catalyst reduced at 500 °C remains quite active with 70% citral conversion after 60 min reaction time.

All the Pt/*y*%Ti–Al_2O_3 catalysts (*y* = 0 to 100%) reduced at 300 °C present very low unsaturated alcohols selectivities, comprised between 5 and 12% at 40% citral conversion (Fig. 5). An increase in UA selectivity is observed after reduction at 500 °C, with a more or less extend according to the titanium content. Indeed, for *y* equal to 10%, the UA selectivity growths only from 6 to 10%, but for 20 and 33% Ti contents, selectivity values of 35 and 50% are obtained, respectively. Then, an appropriated Ti content introduced in alumina oxide allows promoting the selective hydrogenation of the C=O bond of citral compared to Pt sample deposited on pure alumina. The UA selectivities obtained on these Pt/*y*%Ti–Al_2O_3 systems can be comparable or even superior to that of the Pt/TiO_2 P25 reference sample (S_{UA} = 45% after reduction at 500 °C). The beneficial effect of the reduction at high temperature observed on the UA selectivity is then related to the existence of a SMSI effect, knowing that the formed $TiO_{(2-x)}$ ($x < 2$) species can participate to the activation of the C=O bond [22]. Such metal–support interaction can then be maximized through the titanium content in the support.

The Pt/10%Ti–Al_2O_3 mesoporous catalyst reduced at 300 °C was modified by addition of various amounts of germanium using a surface redox reaction (catalytic reduction method), this way of preparation being known to favor the metal–metal interaction in the bimetallic systems [21,25,28]. After preparation, the bimetallic Pt–*x* wt.% Ge/10%Ti–Al_2O_3 (*x* = 1, 2, and 2.5 wt.% deposited Ge) catalysts were reduced *in situ* at 300 °C before their transfer to the citral hydrogenation autoclave. Fig. 6 displays the citral conversion after 60 min reaction time and the selectivity to unsaturated alcohols at isoconversion (40%) obtained on the Pt-Ge/10%Ti–Al_2O_3 systems compared to the Pt/10%Ti–Al_2O_3 parent one. After Ge addition, the citral conversion decreases. The citral conversion is progressively decreasing with the Ge content increase, and a conversion value equal to only 10% is obtained after 60 min reaction time for 2.5 wt.% Ge deposited. This conversion drop after introduction of the Ge modifier was also observed on classical Pt-Ge/TiO_2 catalysts prepared by catalytic reduction and tested previously for citral hydrogenation [22]. This phenomenon is consistent with a poisoning of a part of the Pt active surface by Ge species inactive for hydrogen activation.

In addition to the catalytic activity decrease, the Ge addition to Pt/10%Ti–Al_2O_3 catalyst reduced at 300 °C allows improving the selectivity of the reaction toward unsaturated alcohols (nerol and geraniol) (Fig. 6). Indeed, the UA selectivity increases to a maximum value of approximately 50% for 2 wt.% Ge, before to decrease to 35% for the highest Ge content due to the formation of secondary products (isopulegol and acetals) in higher quantities. Then, the addition of Ge onto Pt allows shifting the reaction selectivity toward the formation of indented α,β-unsaturated alcohols, as previously the reduction at 500 °C after the Pt/*y*%Ti–Al_2O_3 preparation. Previously, the existence of the SMSI effect was proposed to explain the increase of the UA selectivity on the Pt/*y*%Ti–Al_2O_3 catalysts reduced at 500 °C, with the formation of $TiO_{(2-x)}$ ($x < 2$) species that activate the C=O bond of citral. In the same way, on the bimetallic Pt-Ge/TiO_2 catalysts, the presence of oxidized Ge species onto the platinum or in its close vicinity promotes the activation of the carbonyl function by fixing selectively the oxygen atoms of the C=O group. Indeed, in previous studies describing the characterization

of alumina or titania supported Rh-Ge and Pt-Ge bimetallic samples prepared also by the catalytic reduction method [21,22,28], temperature programmed reduction experiments clearly showed the presence of H_2 consumption peaks attributed to the reduction of Ge species (in contact with Rh or Pt, or isolated on the support) but that consumption never corresponded to the entire reduction of Ge entities until a metallic state.

Finally, the addition of 2 wt.% Ge on the Pt/10%Ti–Al_2O_3 catalyst reduced at 300 °C allows obtaining a system as selective toward UA formation as the previous Pt/33%Ti–Al_2O_3 sample after reduction at 500 °C, with besides comparable citral conversions after 60 min reaction time (22–25%). Consequently, in order to achieve higher UA selectivities, Pt/Al_2O_3 catalysts can be modified either by Ti incorporation or by Ge addition provided that to use an appropriate modifier's content and reduction temperature.

4. Conclusion

1.0 wt.% Pt/*y*%Ti–Al_2O_3 (with $y = 10$, 20 and 33%$_{atom}$) materials were studied with the following objectives: (i) to investigate the SMSI effect generated by reduction at high temperature (500 °C) on these original materials, and (ii) to determine the influence of the Ge addition on the catalytic performances of these Pt-based systems. The characterization techniques showed that the as-synthesized materials present a mesopore structure with high BET surface area and mesopore volume. The SMSI effect evaluated using a structure insensitive model reaction, *i.e.* the cyclohexane dehydrogenation, was observed to be more important on the Pt/*y*%Ti–Al_2O_3 catalysts (with $y = 20$ and 33%) than on a classical Pt sample supported on bulk TiO_2 P25.

For citral hydrogenation, performed at 70 °C under hydrogen pressure (7 MPa), the SMSI effect generated by the increase of reduction temperature leads to an increase of the selectivity toward unsaturated alcohols (UA: nerol and geraniol) compared to a Pt catalyst supported on pure alumina, reaching similar values than over Pt/TiO_2 P25 sample. Nevertheless, the citral conversions obtained on the Pt/*y*%Ti–Al_2O_3 materials remain lower than the one obtained on Pt/TiO_2 P25 catalyst, for a same reduction temperature. Ge addition, introduced by catalytic reduction onto the Pt/10%Ti–Al_2O_3 catalyst, also leads to an increase of the UA selectivity during the citral hydrogenation.

Then, the as-prepared Pt/*y*%Ti–Al_2O_3 catalysts are able to generate reactive $TiO_{(2-x)}$ ($x < 2$) species after reduction at high temperature (500 °C), leading to a SMSI effect comparable or superior to that on Pt supported on bulk titania. Moreover, these materials can be modified by Ge addition, the generated partially oxidized Ge species participating also to the activation of the C=O bond. To conclude, this work allows confirming results obtained previously in the literature on various catalytic systems [12–14,22,49,50], *i.e.* that two main routes are efficient to modify properties of noble metal active sites to maximize selectivities toward unsaturated alcohols: (i) support doping and adjustments of the activation conditions and (ii) preparation of bimetallic catalysts.

Acknowledgement

The AUF (Agence Universitaire de la Francophonie) is gratefully acknowledged for the financial support of this work through a 10 month research grant (T. Ekou).

References

[1] K.S.W. Sing, D.H. Everett, R.A.W. Haul, L. Moscou, R.A. Pierotti, J. Rouquerol, T. Siemieniewska, Pure Appl. Chem. 57 (1985) 603.
[2] A. Taguchi, F. Schüth, Micropor. Mesopor. Mater. 77 (2005) 1.
[3] V. Luca, G.J.A.A. Soler-Illia, P.C. Angelomé, P.Y. Steinberg, E. Drabarek, T.L. Hanley, Micropor. Mesopor. Mater. 118 (2009) 443.
[4] N. Krins, M. Faustini, B. Louis, D. Grosso, Chem. Mater. 22 (2010) 6218.
[5] J. Hierso, O. Sel, A. Ringuede, C. Laberty-Robert, L. Bianchi, D. Grosso, C. Sanchez, Chem. Mater. 21 (2009) 2184.
[6] E.V. Rebrov, A. Berenguer-Murcia, B.F.G. Johnson, J.C. Schouten, Catal. Today 138 (2008) 210.
[7] X. He, D. Antonelli, Angew. Chem. Int. Ed. 41 (2002) 214.
[8] F. Schüth, Chem. Mater. 13 (2001) 3184.
[9] A. Sayari, P. Liu, Micropor. Mater. 12 (1997) 149.
[10] W.H. Zhang, J. Lu, B. Han, M. Li, J. Xiu, P. Ying, C. Li, Chem. Mater. 14 (2002) 3413.
[11] S.A. Bagshaw, T.J. Pinnavaia, Angew. Chem. Int. Ed. 35 (1996) 1102.
[12] A.M. Silva, O.A.A. Santos, M.J. Mendes, E. Jordão, M.A. Fraga, Appl. Catal. A 241 (2003) 155.
[13] H. Rojas, G. Borda, P. Reyes, J.J. Martínez, J. Valencia, J.L.G. Fierro, Catal. Today 133–135 (2008) 699.
[14] Z.R. Ismagilov, E.V. Matus, A.M. Yakutova, L.N. Protasova, I.Z. Ismagilov, M.A. Kerzhentsev, E.V. Rebrov, J.C. Schouten, Catal. Today 147S (2009) S81.
[15] M. Bonne, P. Samoila, T. Ekou, C. Especel, F. Epron, P. Marécot, S. Royer, D. Duprez, Catal. Commun. 12 (2010) 86.
[16] P. Gallezot, D. Richard, Catal. Rev. Sci. Eng. 40 (1998) 81.
[17] T.B.L.W. Marinelli, S. Nabuurs, V. Ponec, J. Catal. 151 (1995) 431.
[18] U.K. Singh, M.A. Vannice, Study Surf. Sci. Catal. 130 (2000) 497.
[19] F.V. Wells, M. Billot, Perfumery Technology, E. Horwood Publishers, Chichester, 1981.
[20] S. Galvano, C. Milone, A. Donato, G. Neri, R. Pietropaolo, Catal. Lett. 18 (1993) 349.
[21] T. Ekou, A. Vicente, G. Lafaye, C. Especel, P. Marecot, Appl. Catal. A 314 (2006) 64.
[22] T. Ekou, A. Vicente, G. Lafaye, C. Especel, P. Marecot, Appl. Catal. A 314 (2006) 73.
[23] N. Mahata, F. Gonçalves, M.F.R. Pereira, J.L. Figueiredo, Appl. Catal. A 339 (2008) 159.
[24] T. Ekou, C. Especel, S. Royer, Catal. Today 173 (2011) 44.
[25] G. Lafaye, C. Micheaud-Especel, C. Montassier, P. Marécot, Appl. Catal. A 230 (2002) 19.
[26] A. Douidah, P. Marécot, S. Labruquère, J. Barbier, Appl. Catal. A 210 (2001) 111.
[27] J.P. Brunelle, Pure Appl. Chem. 50 (1978) 1211.
[28] G. Lafaye, T. Ekou, C. Micheaud-Especel, C. Montassier, P. Marécot, Appl. Catal. A 257 (2004) 107.
[29] S.J. Gregg, K.S. Sing, Adsorption Surface Area and Porosity, 2nd ed., Academic Press, New York, 1982.
[30] D. Margolese, J.A. Melero, S.C. Christiansen, B.F. Chmelka, G.D. Stucky, Chem. Mater. 12 (2000) 2448.
[31] T. Sen, G.J.T. Tiddy, J.L. Casci, M.W. Anderson, Chem. Commun. 9 (2003) 2182.
[32] H. Zhu, D.J. Jones, J. Zajac, R. Dutartre, M. Rhomari, J. Roziere, Chem. Mater. 14 (2002) 4886.
[33] T. Ekou, L. Ekou, A. Vicente, G. Lafaye, S. Pronier, C. Especel, P. Marécot, J. Mol. Catal. A 337 (2011) 82.
[34] C.C. Chien, W.P. Chuang, T.T. Huang, Appl. Catal. A 131 (1995) 73.
[35] N.S. De Resende, J.G. Eon, M. Schmal, J. Catal. 183 (1999) 6.
[36] I.H. Cho, S.B. Park, S.J. Cho, R. Ryoo, J. Catal. 173 (1998) 295.
[37] J.A. Cusumano, G.W. Dembinski, J.H. Sinfelt, J. Catal. 5 (1966) 471.
[38] D.W. Blakely, G.A. Somorjai, J. Catal. 42 (1976) 181.
[39] I. Rodriguez-Ramos, A. Guerrero-Ruiz, J. Catal. 135 (1992) 458.
[40] C.L. Pieck, P. Marecot, J.M. Parera, J. Barbier, Appl. Catal. A 126 (1995) 153.
[41] A. Vicente, T. Ekou, G. Lafaye, C. Especel, P. Marécot, C.T. Williams, J. Catal. 275 (2010) 202.
[42] P. Mäki-Arvela, L.P. Tiainen, A.K. Neyestanaki, R. Sjöholm, T.K. Rantakylä, E. Laine, T. Salmi, D.Y. Murzin, Appl. Catal. A 237 (2002) 181.
[43] U.K. Singh, M.A. Vannice, J. Catal. 199 (2001) 73.
[44] N.F. Brown, M.A. Barteau, J. Am. Chem. Soc. 114 (1992) 4258.
[45] C.J. Houtman, M.A. Barteau, J. Catal. 130 (1991) 528.
[46] E.L. Rodriguez, J.M.C. Bueno, Appl. Catal. A 232 (2002) 147.
[47] S. Nishiyama, T. Hara, S. Tsuruya, M. Masai, J. Phys. Chem. B 103 (1999) 4431.
[48] U.K. Singh, M.A. Vannice, J. Catal. 191 (2000) 165.
[49] U.K. Singh, M.A. Vannice, J. Mol. Catal. A 163 (2000) 233.
[50] L.N. Protasova, E.V. Rebrov, T.S. Glazneva, A. Berenguer-Murcia, Z.R. Ismagilov, J.C. Schouten, J. Catal. 271 (2010) 161.